Biallelic Mutations in Citron Kinase Link Mitotic Cytokinesis to Human Primary Microcephaly

Hongda Li,[1,2] Stephanie L. Bielas,[1,2,3] Maha S. Zaki,[4] Samira Ismail,[4] Dorit Farfara,[1,2] Kyongmi Um,[1,2] Rasim O. Rosti,[1,2] Eric C. Scott,[1,2] Shu Tu,[5] Neil C. Chi,[5] Stacey Gabriel,[6] Emine Z. Erson-Omay,[7] A. Gulhan Ercan-Sencicek,[7] Katsuhito Yasuno,[7] Ahmet Okay Çağlayan,[8] Hande Kaymakçalan,[9] Barış Ekici,[9] Kaya Bilguvar,[7] Murat Gunel,[7,*] and Joseph G. Gleeson[1,2,*]

Cell division terminates with cytokinesis and cellular separation. Autosomal-recessive primary microcephaly (MCPH) is a neurodevelopmental disorder characterized by a reduction in brain and head size at birth in addition to non-progressive intellectual disability. MCPH is genetically heterogeneous, and 16 loci are known to be associated with loss-of-function mutations predominantly affecting centrosomal-associated proteins, but the multiple roles of centrosomes in cellular function has left questions about etiology. Here, we identified three families affected by homozygous missense mutations in *CIT*, encoding citron rho-interacting kinase (CIT), which has established roles in cytokinesis. All mutations caused substitution of conserved amino acid residues in the kinase domain and impaired kinase activity. Neural progenitors that were differentiated from induced pluripotent stem cells (iPSCs) derived from individuals with these mutations exhibited abnormal cytokinesis with delayed mitosis, multipolar spindles, and increased apoptosis, rescued by CRISPR/Cas9 genome editing. Our results highlight the importance of cytokinesis in the pathology of primary microcephaly.

Primary microcephaly is characterized by reduced head size accompanied by variable degrees of intellectual, language, and motor-skill disability, but not progressive cognitive decline, spasticity, or epilepsy.[1] In autosomal-recessive primary microcephaly (MCPH [MIM: 251200]), the cerebral cortex is particularly reduced in size, leading to an apparently "simplified gyral pattern" because mantle thickness is grossly preserved but surface area is dramatically reduced.[2] MRI of an affected fetus with a prenatal diagnosis has shown the frontal lobes of the cerebral cortex to be affected as early as 30 weeks of gestation.[3]

MCPH is considered a disorder of neural progenitor cell (NPC) proliferation or survival during embryogenesis, predominantly of autosomal-recessive or X-linked inheritance. Mutations in 16 loci (MCPH1–MCPH16) have been described as associated with MCPH, and many of these loci encode proteins implicated in the biogenesis and function of the centrosome, an organelle critical for multiple cellular functions.[4] MCPH-associated genes encode essential centrosomal-duplication proteins—SAS-6, STIL, CPAP, CEP63, CEP135, and CEP152—and pericentriolar-matrix proteins—WDR62, ASPM, and CEP215 (also known as CDK5Rap2). Most of these mutations generate premature stop codons that predominantly result in nonsense-mediated mRNA decay and absent proteins. *ASPM* (MIM: 605481) mutations, which result in alterations in mitotic-spindle regulation, account for approximately 40% of MCPH cases.[1] Recently, a hierarchy of MCPH-associated proteins co-recruiting to the centrosome was described as mediating centrosomal duplication,[5] suggesting a critical role for these MCPH-associated proteins in centrosomal biogenesis.

Because centrosomes play multiple roles in the cell (e.g., serving as microtubule-organizing centers, as spindle poles during mitosis, and as basal bodies in ciliogenesis), the cellular etiology of MCPH has remained unclear. Initial studies focused on the roles of MCPH-associated proteins at the spindle pole in determining mitotic-spindle orientation. The position of the centrosome in the dividing cell regulates mitotic orientation, which can, in turn, regulate neural stem cell fate decisions.[6] Indeed, defects in the orientation of the mitotic cleavage plane contribute to neurogenesis defects in an MCPH model.[7] Recent work has extended the roles of centrosomes in microcephaly to include a potential function in cilia. MCPH-associated proteins play essential roles in cilia, which are critical for cells to process Sonic hedgehog signals that can regulate neurogenesis.[8] Furthermore, cells harboring mutations in microcephaly-associated genes can show disrupted ciliogenesis,[9,10] but classically, ciliopathy disorders do not demonstrate microcephaly. Thus, identifying non-centrosomal factors that lead to MCPH when mutated could help clarify mechanisms.

[1]Howard Hughes Medical Institute, Rady Children's Institute of Genomic Medicine, University of California, San Diego, San Diego, CA 92093, USA; [2]Laboratory for Pediatric Brain Disease, The Rockefeller University, New York, NY 10065, USA; [3]Department of Human Genetics, School of Medicine, University of Michigan, Ann Arbor, 48109 MI, USA; [4]Clinical Genetics Department, Human Genetics and Genome Research Division, National Research Centre, Cairo 12311, Egypt; [5]Division of Cardiology, Department of Medicine, University of California, San Diego, San Diego, CA 92093, USA; [6]Broad Institute of MIT and Harvard, Cambridge, MA 02141, USA; [7]Yale Program on Neurogenetics, Departments of Neurosurgery, Neurobiology, and Genetics, School of Medicine, Yale University, New Haven, CT 06510, USA; [8]Department of Medical Genetics, School of Medicine, Istanbul Bilim University, Istanbul 34394, Turkey; [9]Department of Pediatrics, Istanbul Bilim University, Istanbul 34394, Turkey
*Correspondence: murat.gunel@yale.edu (M.G.), jogleeson@ucsd.edu (J.G.G.)
http://dx.doi.org/10.1016/j.ajhg.2016.07.004.

To identify additional mechanisms of microcephaly, we recruited individuals displaying MCPH in the setting of parental consanguinity. Subjects were enrolled according to protocols approved by institutional review boards at affiliated institutions. We performed whole-exome sequencing (WES) on at least one affected member per family and focused on the identification of potentially deleterious rare homozygous variants.[11] Three independent consanguineous families whose children showed non-syndromic MCPH presented with homozygous missense variants in *CIT* (MIM: 605629), encoding citron rho-interacting kinase (CIT), which has established roles in cytokinesis. The variants were unique in our dataset of more than 5,000 geographically matched individuals sequenced by exome, were not represented in the Greater Middle Eastern Variome or the Exome Aggregation Consortium (ExAC) Browser, were fully segregated in the families according to a recessive mode of inheritance (Figure S1A), and were predicted to be damaging with altered evolutionarily conserved amino acids (Figure S1B and Table S1). Moreover, none of the families displayed functionally relevant variants in any of the previously established MCPH-associated genes in OMIM, and no other variants that met screening criteria showed segregation according to a recessive fully penetrant mode of inheritance (Table S1).

Family 718 from Egypt had four children affected by MCPH from a consanguineous marriage (Figure 1A and Table 1). Individual 718-IV-1 was born at full term with a reduced head circumference (HC) of 32.5 cm (−1 SD) and an average body weight. Developmental delay with motor, speech, and social impairment was noted at 3 years. At 9 years, HC was 44.8 cm (−5.6 SDs). He displayed a sloping forehead (Figure 1B), moderate intellectual disability, mild hypertonia, and brisk reflexes. His sister (718-IV-2) had a similar clinical course and had a HC of 43 cm (−7.4 SDs) at 8 years of age. Similarly, 718-IV-3 was noted to have microcephaly at birth but died on the first day of life as a result of unrelated causes, and 718-IV-4 had a HC of 41 cm (−5.6 SDs) at age 2 years and mild intellectual disability. Clinical features were not progressive, and no spasticity or epileptic seizures were described. Brain MRI of 718-IV-1, 718-IV-2, and 718-IV-4 revealed a simplified gyral pattern and a thin corpus callosum (Figure 1B). WES identified a homozygous missense variant (c.317G>T [p.Gly106Val]; hg19 chr12: g.120295424C>A; GenBank: NM_001206999.1) affecting the kinase domain of CIT (Figures 1C and 1D).

Family 1379 from Egypt had two first-cousin parental consanguineous branches and three children affected by MCPH. All exhibited reduced head size, intellectual disability, delayed motor and speech development, hypertonia, brisk reflexes, sloping foreheads, and relatively large ears. HC was −7 to −8.4 SDs in the first decade of life. MRI of individual 1379-IV-B1-1 demonstrated a simplified gyral pattern and a thin corpus callosum, similar to those in family 718. WES revealed a homozygous missense variant (c.376A>C [p. Lys126Gln]; hg19 chr12: g.120295365T>G) also affecting the kinase domain. We noticed that subject 1379-B1-1 was more severely impaired than other affected individuals from this family. Whether other variants from this individual (Table S2) contribute to his clinical symptoms requires further investigation.

Family 1924 from Turkey had a single male child affected with MCPH from a consanguineous marriage. He displayed a reduced HC of 45 cm (−6.5 SDs), intellectual disability, delayed motor and speech development, and large protruding ears. WES detected a homozygous variant (c.689A>T [p.Asp230Val]; hg19 chr12: g.120270639T>A) also affecting the encoded kinase domain. It is worth noting that another common feature of the MCPH-affected individuals from these three families is short stature, which is also seen in individuals with *MCPH1* mutations[12] but is not a common finding in other MCPH cases.

CIT was identified as a 183 kDa GTP-bound Rac and Rho binding protein.[13] There are two cDNA isoforms: (1) one (GenBank: NM_001206999.1) encoding a 2,027 aa full-length CIT-K, which has N-terminal kinase, coiled-coil, zinc finger, Pleckstrin homology, and citron homology domains,[14] and (2) another (GenBank: NM_007174.2) encoding a 1,545 aa CIT-N, which is produced by alternative transcriptional initiation and lacks the kinase domain but maintains the other C-terminal domains (Figures 1C and 1D).[15] *CIT-K* mRNA is specifically expressed in proliferating neural precursors in the developing brain, whereas *CIT-N* mRNA is expressed by post-mitotic cells,[16] suggesting a role for the kinase in neurogenesis. CIT-K localizes to the cleavage furrow and midbody, where it promotes cytokinesis during cell division.[17]

The *CIT* variants that we identified were notable for several reasons. First, variants were not observed in the ExAC Browser or in our collective ethnically matched database of 10,000 WES traces from families affected by neurodevelopmental disease. Second, all variants occurred within the kinase domain of the protein. Third, all variants altered highly conserved residues, not just in evolutionarily orthologs of CIT but also in other sequence-similar kinase family members, including ROCK1 and AKT1 (Figure S1C). In fact, p.Lys126Gln, the amino acid substitution detected in family 1379, was in the invariant lysine (K) residue in subdomain II, which is present in all known kinases and is involved in the phosphotransfer reaction.[18] Fourth, using the resolved structure of the ROCK1 kinase domain to predict the function of the altered amino acids in CIT,[19] we found that two variants (p.Gly106Val and p.Lys126Gln) were within the ATP binding pocket of the kinase domain, and one (p.Asp230Val) was within the DFG (Asp-Phe-Gly) motif, which positions ATP for phosphoryl transfer[20] (Figure S1D). These findings suggest that the mutations impair kinase activity.

To test for impaired kinase activity, we FLAG tagged amino acids 1–480 of CIT-K, encoding the kinase domain, either as wild-type (WT) or with each identified *CIT* variant engineered. The tagged proteins were immunoprecipitated

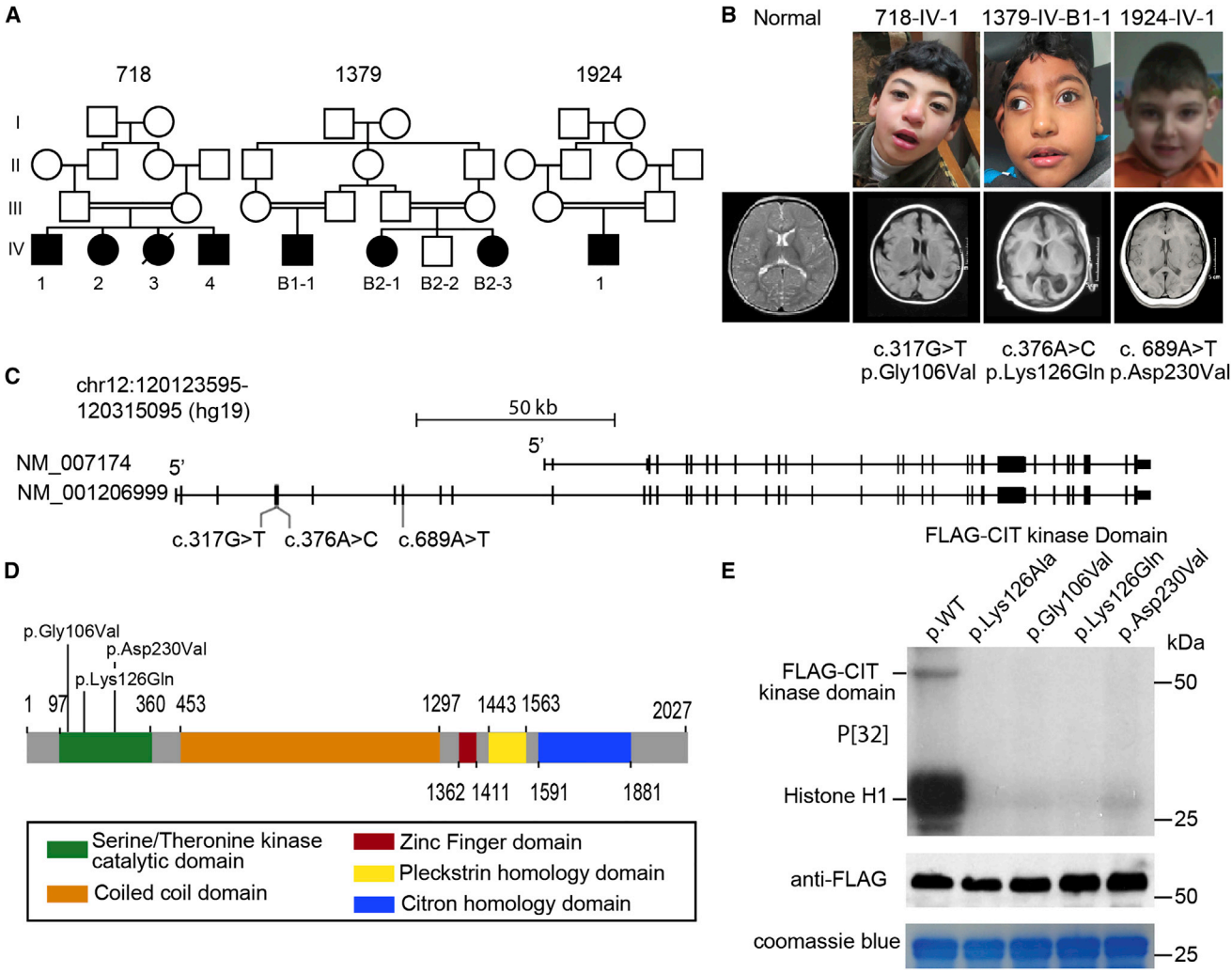

Figure 1. Mutations in *CIT* Cause Primary Microcephaly

(A) Pedigrees of consanguineous families 718, 1379, and 1924. Symbols are as follows: filled, affected; empty, unaffected; circle, female; square, male; hash, deceased; B, branch.

(B) Faces (top) and axial MRI (bottom) of representative affected individuals from each family show reduced brain volume and a simplified gyral pattern, consistent with a diagnosis of MCPH.

(C) Exonic structure of *CIT* and the location of the identified mutations. The shorter CIT-N isoform, encoded by GenBank: NM_007174.2, lacks the N-terminal kinase domain. The longer CIT-K isoform, encoded by GenBank: NM_001206999.1, encodes the kinase domain where the *CIT* variants localize.

(D) Identified missense variants cluster within the kinase domain of full length CIT-K.

(E) Defective activity of the kinase domain with CIT variants. P[32] incorporation was detected in the wild-type only for histone H1 and FLAG-CIT autophosphorylation.

from transfected 293T cells with anti-FLAG antibody and then used in an in vitro kinase assay. We utilized a kinase-dead (p.Lys126Ala) version with an alanine substitution at the ATP donor site as a negative control.[17] As reported, WT CIT-K exhibited kinase activity toward exogenous histone H1 substrate, as well as autophosphorylation activity.[21] Neither of these kinase activities was observed from the clone harboring p.Lys126Ala. Furthermore, none of the clones with *CIT* variants showed phosphorylation of histone H1 or autophosphorylation on the basis of P[32] incorporation (Figure 1E), suggesting that all three variants impair kinase activity.

Cytokinesis refers to the final stage of the cell cycle, in which the physical separation of two daughter cells occurs during cell division. During cytokinesis, the contractile ring forms beneath the cell equatorial surface to form the cleavage furrow, and then ingression of the furrow results in the formation of an intercellular bridge called the midbody. The cell cycle completes as the midbody is resolved and the two daughter cells separate, a process known as abscission.[22] Disrupted cytokinesis frequently leads to binucleated cells, aneuploidy, chromosomal instability, activation of p53, cell-cycle arrest, and apoptosis. CIT-K is localized in the midbody during abscission, and knockdown can result in failed abscission followed by re-fusion of the two daughter cells.[23]

To study the functional consequences of the *CIT* variants at the cellular level, we collected skin-derived fibroblasts

Table 1. Clinical Features of the Affected Individuals in This Study

	718-IV-1	718-IV-2	718-IV-4	1379-IV-B2-1	1379-IV-B2-3	1379-IV-B1-1	1924-IV-1
Gender	male	female	male	female	female	male	male
Ethnic origin	Egypt	Egypt	Egypt	Egypt	Egypt	Egypt	Turkey
Pregnancy duration	term	term	term	term	term	term	term
Weight at birth	3.2 kg (−0.2 SD)	3 kg (−0.4 SD)	3.5 kg (+0.1 SD)	2.5 kg (−1.9 SDs)	2.5 kg (−1.9 SDs)	2 kg (−2.4 SDs)	NA
Length at birth	48 cm (−0.4 SD)	49 cm	50 cm (+0.4 SD)	50 cm (+0.4 SD)	49 cm	49.5 cm (+0.2 SD)	NA
HC at birth	31 cm	31.5 cm	32 cm	31 cm	30 cm	30 cm	NA
HC at last examination	44.8 cm (−5.6 SDs)	43 cm (−7.4 SDs)	41 cm (−5.6 SDs)	41.2 cm (−7.8 SDs)	40 cm (−8.4 SDs)	39.5 cm (−8.3 SDs)	45 cm (−6.5 SDs)
Diagnosis age	3 years	2 years	at birth	5 years	1 year	1 year	4 years
Intellectual disability	moderate	mild	mild	moderate	moderate	severe	moderate
Development							
Gross motor	delayed	delayed	delayed	delayed	delayed	delayed	delayed
Fine motor	delayed	delayed	normal	delayed	delayed	absent	delayed
Language	delayed	delayed	delayed	delayed	delayed	absent	delayed
Social	delayed	delayed	delayed	delayed	delayed	delayed	delayed
Seizures							
Present	–	–	–	–	–	–	–
Neurological Findings							
Hypertonia	mild	mild	–	mild	mild	severe, acquired arthrogryposis	–
Hypotonia	–	–	–	–	–	–	–
Deep tendon reflexes	brisk	brisk	normal	brisk	brisk	brisk	normal
Spastic tetraplegia	–	–	–	–	–	+	–
Ataxia	–	–	–	–	–	–	–
Investigations							
Metabolic	normal	normal	NA	NA	NA	normal	normal
VEP and ERG	normal	normal	normal	NA	NA	normal	normal
EEG	normal	normal	normal	NA	NA	generalized epileptogenic activity	normal
MRI							
Simplified gyral pattern	+	+	+	NA	NA	+	+

(*Continued on next page*)

Table 1. *Continued*

	718-IV-1	718-IV-2	718-IV-4	1379-IV-B2-1	1379-IV-B2-3	1379-IV-B1-1	1924-IV-1
Hypogenesis of corpus callosum	+	+	+	NA	NA	+	–
Cerebellar hypoplasia	–	–	–	NA	NA	–	–
Brainstem hypoplasia	–	–	–	NA	NA	–	–
White-matter abnormalities	–	–	–	NA	NA	–	+
Miscellaneous							
Short stature	125 cm (–1 SD)	119 cm (–1.2 SDs)	86 cm (mean)	124 cm (–1.5 SDs)	102 cm (–1.2 SDs)	104 cm (–0.9 SD)	NA
Optic atrophy	–	–	–	–	–	–	NA
Autistic features	–	–	–	–	–	mild	NA
Dysmorphism	sloping forehead, tubular nose, full lips and cheeks, large ears	sloping forehead, tubular nose, full lips and cheeks, large ears	sloping forehead, tubular nose, full lips and cheeks, large ears	sloping forehead, tubular nose, full lips and cheeks, large ears	sloping forehead, tubular nose, full lips and cheeks, large ears	flat occiput, esotropia (R), large ears, retruded mandible, full lips and cheeks, tubular nose	low anterior hairline, full lips, large ears

Abbreviations are as follows: EEG, electroencephalography; ERG, electroretinography; HC, head circumference; NA, not available; R, right; and VEP, visual evoked potential.

from affected and carrier individuals from families 718 and 1379, from affected individuals from family 1924, and from a healthy unrelated control individual. Primary fibroblasts were unremarkable in culture and displayed no defects in cell proliferation or mitosis (data not shown). Therefore, we generated induced pluripotent stem cells (iPSCs) through reprograming by integration-free episomal methods.[24] We excluded gross chromosomal post-reprogramming rearrangements. Furthermore, we found no defect in differentiation of iPSCs into mesodermal or endodermal lineages.

From iPSCs, we next generated NPCs by using a dual-SMAD inhibition protocol.[25] As expected, amounts of PAX6 and CIT-K in mutant NPCs were comparable to those in related controls (Figures S2A and S2B). CIT-K was detected and localized to the midbody core in a manner indistinguishable from that of the wild-type during cytokinesis (Figure S2C), suggesting that the absence of kinase activity does not lead to protein mislocalization. Furthermore, midbody integrity was intact, as evidenced by indistinguishable localization of Aurora B to the midbody flank.[26]

To assess for functional defects in cytokinesis, we used time-lapse imaging to monitor cell-cycle progression by comparing the entire duration of mitosis in NPCs. Previous work in HeLa cells showed that knockdown of *CIT* resulted in delayed cytokinesis and "blebbing" of the cellular membrane, followed by either "early fusion" or "late fusion" of the daughters with binucleated derivatives.[23] In mutant NPCs, we found a dramatic increase in the length of cytokinesis and cellular blebbing in all mitotic cells recorded. This resulted in one of two outcomes. In about 25% of cells, blebbing was followed by failed cytokinesis and the formation of cellular fusions and binucleated cells (Figure 2A, middle). In the remainder, after the delay, cytokinesis completed with separation of the two daughter cells (Figure 2A, bottom). On average, the length of cytokinesis was doubled in mutant cells (mean ± SEM: 73.6 ± 4.1 min versus 33.5 ± 1.4 min).

Failure to achieve cytokinesis can result in subsequent multipolar spindles as a result of duplicated centrosomes and nuclear material. To evaluate for multipolar spindles, we fixed and stained sub-confluent NPCs for α-tubulin and DAPI and then counted the percentage of mitotic figures with three or more spindle poles. Multipolar spindles were evident in about 28% of mitotic cells, whereas they were evident in fewer than 5% of control cells. We conclude that multipolar spindles are a frequent feature of *CIT*-mutated NPCs.

To test whether the mutation caused the observed cellular phenotypes, we corrected the c.317G>T (p.Gly106Val) mutation by using CRISPR/Cas9-based genome editing in iPSCs derived from affected individual 718-IV-1 by homologous recombination (Figure 3A). A genome-editing donor plasmid containing wild-type *CIT* exon 4, flanking genomic sequence, and a puromycin cassette (LoxP-Puro-LoxP) was electroporated together with Cas9- and gRNA-expressing plasmids into iPSCs.

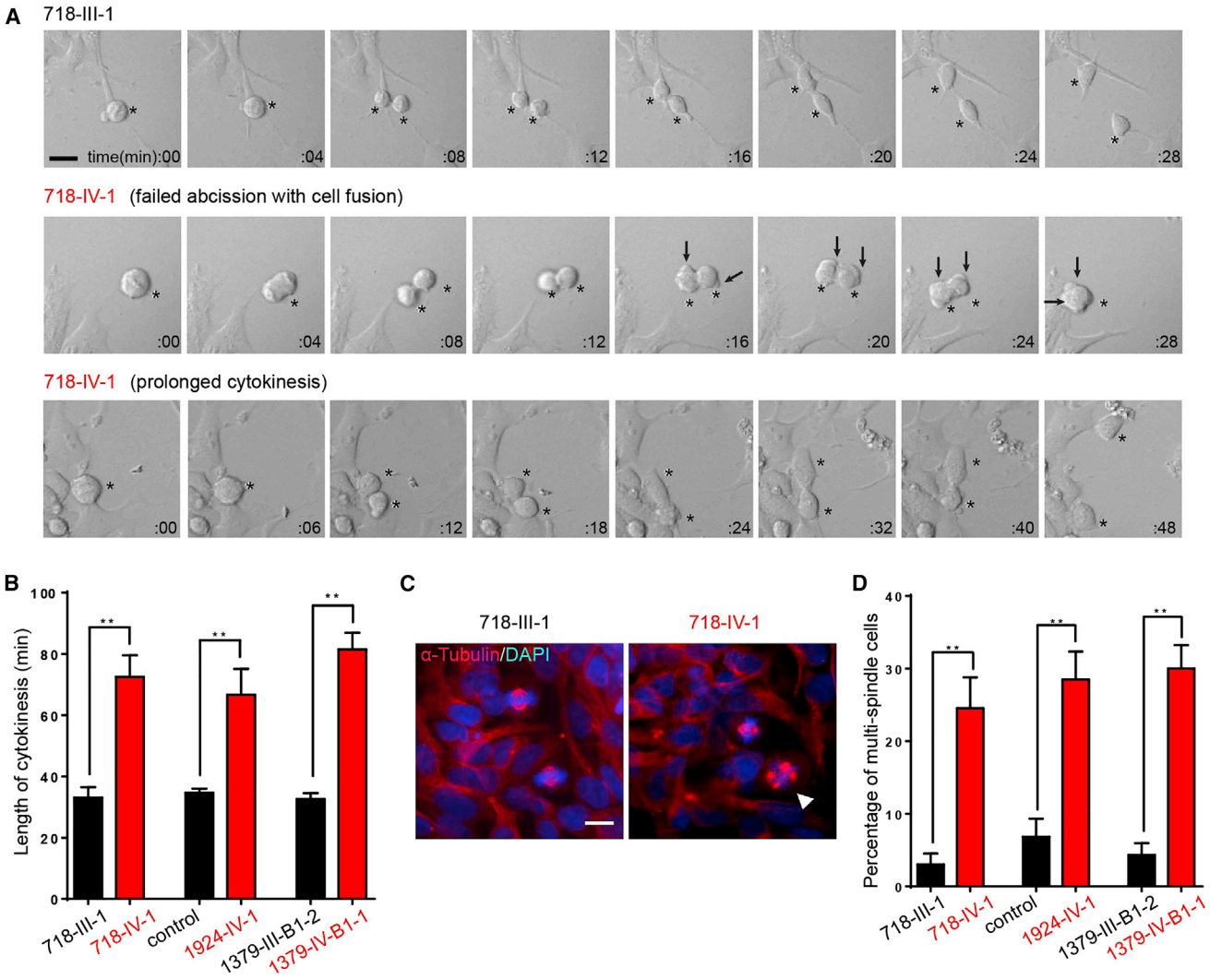

Figure 2. Cell-Division Defects in NPCs Derived from Individuals with *CIT* Variants

(A) Representative phase-contrast time-lapse images of NPCs from unaffected and affected individuals. 718-III-1 is a healthy father (black typeface), and 718-IV-1 is an affected member (red typeface). Asterisks mark the dividing cells analyzed in each series. Note that unaffected cells completed division within 28 min. Affected cells (top row) showed blebbing at 16 min and then incomplete cytokinesis with binucleated derivatives at 28 min. Affected cells (bottom row) showed minimal blebbing and then division by 48 min. Arrows mark cortical blebbing.

(B) Quantification of the length of cytokinesis (n = 15 cells per group).

(C and D) Representative images and quantification of the percentage of multipolar cells in NPCs from unaffected (C) and affected (D) individuals. Arrowheads mark multipolar cells (n = 7 cultures per group).

Bar graphs show the mean ± SEM. **$p < 0.01$ (Student's t test). Scale bar represents 10 μm.

Individual iPSC clones were propagated after puromycin selection. After successful biallelic targeting (Figures S3A–S3C), the puromycin cassette was removed by transfection with a plasmid expressing Cre recombinase (Figure S3D). Of note, the expression level of *CIT* was indistinguishable between affected and wild-type cells after puromycin recombination in corrected lines (data not shown), suggesting that genome editing did not adversely affect expression. We then differentiated cells into NPCs and performed time-lapse microscopy to evaluate cytokinesis. Corrected cells showed no delay in the length of cytokinesis (Figures 3B and 3C). Furthermore, there was no accumulation above baseline of multiple spindle cells in corrected NPCs (Figures 3D and 3E). We conclude that the *CIT* variants identified from the affected individual were necessary for mediating defects in cytokinesis, given that cellular defects were corrected when the wild-type allele was genetically engineered into mutant cells.

Both prolonged and incomplete cell division are associated with genotoxic stress and increased apoptotic cell death[22,27] and are proposed as mechanisms in mouse and zebrafish MCPH models.[28–30] Furthermore, *Cit*-deficient mice display binucleated cells and increased apoptosis in the developing cerebral cortex.[16] To test for apoptosis in a complex cellular milieu, we generated neurospheres from control and mutant cells, together with

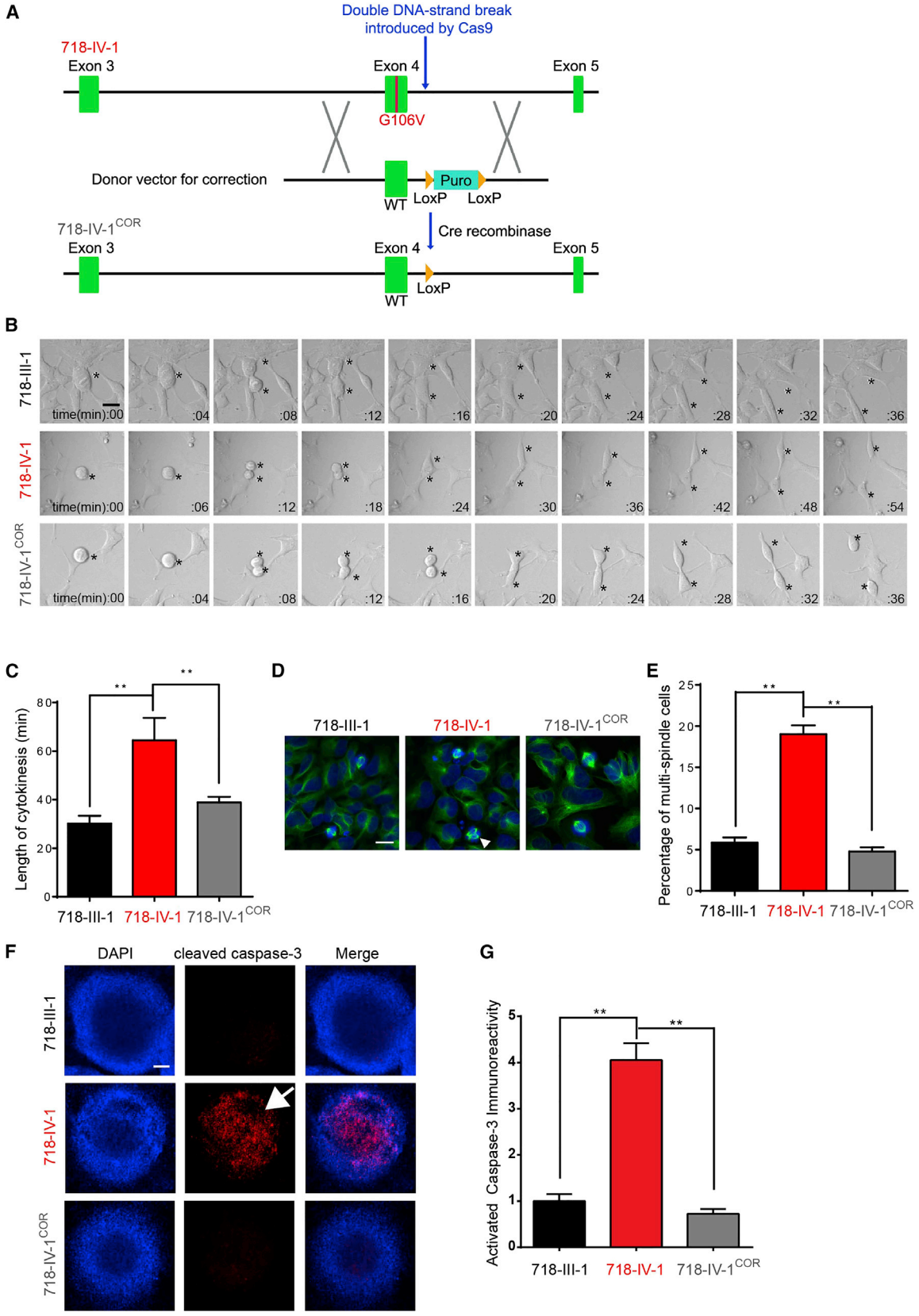

Figure 3. Correcting the *CIT* Variant Rescues Cellular NPC Phenotypes in Cells from Affected Individuals
(A) Schematic of gene-editing strategy for correcting the *CIT* variant in iPSCs. WT exon 4 and the floxed puromycin cassette were recombined at the mutant locus after Cas9 cleavage. Cre-mediated removal of the LoxP-Puro-LoxP cassette left only the single LoxP site.

(legend continued on next page)

CIT-mutation-corrected cells, and then stained for cleaved caspase-3 as a marker of apoptosis. Dramatic evidence for increased apoptosis (an overall 4-fold increase in intensity) was detected in mutant but not control or mutation-corrected neurospheres (Figures 3F and 3G).

Here, we describe families affected by recessive MCPH caused by biallelic missense *CIT* alleles affecting the kinase domain and thus leading to undetectable kinase activity. These mutations were remarkable in that they did not alter the expression level of the mRNA or CIT localization in anaphase, suggesting that the kinase activity of CIT is required for function in controlling cytokinesis. Previous studies using overexpression of kinase-dead CIT in HeLa cells found largely retained effects, but these studies could not differentiate between loss-of-function and toxic gain-of-function effects.[17] The fact that the parent and sibling carriers were healthy and had a normal HC suggests that our mutations did not act in a dominant-negative fashion, and because no individuals with truncating *CIT* mutations were detected with MCPH, it is tempting to speculate that CIT retains some biological activity even in the setting of kinase loss. This is further supported by the finding of the more severe microlissencephaly phenotype observed among individuals with truncating *CIT* mutations, shown in the accompanying paper by Li et al.[31]

CIT is classified as an AGC kinase (by homology with protein kinases A, G, and C), which are regulated by second messengers, such as cyclic AMP (PKA) and lipids (PKC).[32] CIT binds activated Rho and Rac,[13] and activated Rho correlates with the translocation of CIT to the cleavage furrow.[33] Most AGC kinases require sequential phosphorylations of the "turn" and "hydrophobic" motifs to stabilize the active conformation,[34] but it is still unclear whether other kinases regulate CIT's kinase activity. Although CIT can function with proteins such as KIF14 and TUBB3,[26,35] direct phosphorylation targets of CIT have not yet been identified.

Several spindle-pole-localized MCPH-associated proteins, including ASPM, CENPJ, and CDK5RRAP2, are also present in the midbody during cytokinesis.[36] Moreover, loss of ASPM in cultured cells leads to cytokinesis failure followed by apoptosis, in addition to misorientation of the mitotic spindle.[37] Our results confirm that cytokinesis failure and subsequent apoptosis are underlying mechanisms for the genetic forms of MCPH. Interestingly, the C terminus of ASPM interacts with CIT-K, suggesting that CIT-K and ASPM might function together in regulating cytokinesis.[36]

Our data align with those of other studies arguing against MCPH as a primary defect of centrosomes for the following reasons. First, fruit flies without centrosomes still undergo neurogenesis,[38] suggesting that centrosomes are not required for neuronal proliferation. Second, mutations in microcephaly-associated genes *Sas4* and *Cep63* in mice lead to genotoxic stress, activation of the p53 pathway, and apoptosis, probably independent of cleavage plane effects.[39] Third, neurogenesis defects in microcephaly mouse models have been rescued at least in part by concurrent removal of p53.[39,40] The data support a model in at least some forms of microcephaly, whereby loss of mitotic integrity through an effect on centrosomes or cytokinesis can result in genome instability, genotoxic stress, apoptosis, and subsequently, reduced cerebral volume.

Accession Numbers

The WES data for all study subjects who consented to data release have been deposited under accession number dbGaP: phs000288.

Supplemental Data

Supplemental Data include three figures and two tables and can be found with this article online at http://dx.doi.org/10.1016/j.ajhg.2016.07.004.

Acknowledgments

We thank Joseph LoTurco and Ferdinando Di Cunto for communicating unpublished results and Susan Taylor for providing suggestions on the project. We thank the subjects and their families for their contributions to this study. This work was supported by the NIH (R01NS041537, R01NS048453, R01NS052455, and P01HD070494 to N.C.), the Howard Hughes Medical Institute (J.G.G.), and the Druckenmiller Fellowship from the New York Stem Cell Foundation (to H.L). We thank the Broad Institute (U54HG003067 to E. Lander) and the Yale Center for Mendelian Disorders (U54HG006504 to R. Lifton) for sequencing support.

Received: May 1, 2016
Accepted: July 5, 2016
Published: July 21, 2016

Web Resources

dbGaP, http://www.ncbi.nlm.nih.gov/gap
Exome Aggregation Consortium (ExAC) Browser, http://exac.broadinstitute.org/

(B) Representative differential interference contrast (DIC) time-lapse images from unaffected (black), affected (red), and mutation-corrected (gray) NPCs during cytokinesis. Scale bar represents 10 μm.
(C) Quantification of the length of cytokinesis (n = 15 cells for each group).
(D and E) Representative images and quantification of the percentage of multipolar cells in unaffected, affected, and mutation-corrected (COR) NPCs. Arrowheads mark multipolar cells (n = 4 cultures per group). Scale bar represents 10 μm.
(F and G) Representative images (F) and quantification (G) of active caspase-3 immunoreactivity in unaffected, affected, and mutation-corrected neurospheres (n = 6 cultures per group). Note the dramatically increased amount of cleaved caspase-3 in mutant cells (718-IV-1) prior to correction (F, arrow). Scale bar represents 150 μm.
(C, E, and G) One-way ANOVA was followed by Tukey's multiple-comparison test.
Bar graphs show the mean ± SEM. **$p < 0.01$.

Greater Middle East Variome, http://igm.ucsd.edu/gme
NHLBI Exome Sequencing Project (ESP) Exome Variant Server, http://evs.gs.washington.edu/EVS/
OMIM, http://www.omim.org/
PolyPhen-2, http://genetics.bwh.harvard.edu/pph2/
PROVEAN, http://provean.jcvi.org/
RefSeq, http://www.ncbi.nlm.nih.gov/refseq/
SeattleSeq, http://snp.gs.washington.edu/SeattleSeqAnnotation137/
SIFT, http://sift.jcvi.org/

References

1. Faheem, M., Naseer, M.I., Rasool, M., Chaudhary, A.G., Kumosani, T.A., Ilyas, A.M., Pushparaj, P., Ahmed, F., Algahtani, H.A., Al-Qahtani, M.H., and Saleh Jamal, H. (2015). Molecular genetics of human primary microcephaly: an overview. BMC Med. Genomics *8* (*Suppl 1*), S4.
2. Adachi, Y., Poduri, A., Kawaguch, A., Yoon, G., Salih, M.A., Yamashita, F., Walsh, C.A., and Barkovich, A.J. (2011). Congenital microcephaly with a simplified gyral pattern: associated findings and their significance. AJNR Am. J. Neuroradiol. *32*, 1123–1129.
3. Desir, J., Cassart, M., David, P., Van Bogaert, P., and Abramowicz, M. (2008). Primary microcephaly with ASPM mutation shows simplified cortical gyration with antero-posterior gradient pre- and post-natally. Am. J. Med. Genet. A. *146A*, 1439–1443.
4. Woods, C.G., and Basto, R. (2014). Microcephaly. Curr. Biol. *24*, R1109–R1111.
5. Kodani, A., Yu, T.W., Johnson, J.R., Jayaraman, D., Johnson, T.L., Al-Gazali, L., Sztriha, L., Partlow, J.N., Kim, H., Krup, A.L., et al. (2015). Centriolar satellites assemble centrosomal microcephaly proteins to recruit CDK2 and promote centriole duplication. eLife *4*, 4.
6. Kaltschmidt, J.A., Davidson, C.M., Brown, N.H., and Brand, A.H. (2000). Rotation and asymmetry of the mitotic spindle direct asymmetric cell division in the developing central nervous system. Nat. Cell Biol. *2*, 7–12.
7. Fish, J.L., Kosodo, Y., Enard, W., Pääbo, S., and Huttner, W.B. (2006). Aspm specifically maintains symmetric proliferative divisions of neuroepithelial cells. Proc. Natl. Acad. Sci. USA *103*, 10438–10443.
8. Tong, C.K., Han, Y.G., Shah, J.K., Obernier, K., Guinto, C.D., and Alvarez-Buylla, A. (2014). Primary cilia are required in a unique subpopulation of neural progenitors. Proc. Natl. Acad. Sci. USA *111*, 12438–12443.
9. Waters, A.M., Asfahani, R., Carroll, P., Bicknell, L., Lescai, F., Bright, A., Chanudet, E., Brooks, A., Christou-Savina, S., Osman, G., et al. (2015). The kinetochore protein, CENPF, is mutated in human ciliopathy and microcephaly phenotypes. J. Med. Genet. *52*, 147–156.
10. Hu, W.F., Pomp, O., Ben-Omran, T., Kodani, A., Henke, K., Mochida, G.H., Yu, T.W., Woodworth, M.B., Bonnard, C., Raj, G.S., et al. (2014). Katanin p80 regulates human cortical development by limiting centriole and cilia number. Neuron *84*, 1240–1257.
11. Dixon-Salazar, T.J., Silhavy, J.L., Udpa, N., Schroth, J., Bielas, S., Schaffer, A.E., Olvera, J., Bafna, V., Zaki, M.S., Abdel-Salam, G.H., et al. (2012). Exome sequencing can improve diagnosis and alter patient management. Sci. Transl. Med. *4*, 138ra78.
12. Neitzel, H., Neumann, L.M., Schindler, D., Wirges, A., Tönnies, H., Trimborn, M., Krebsova, A., Richter, R., and Sperling, K. (2002). Premature chromosome condensation in humans associated with microcephaly and mental retardation: a novel autosomal recessive condition. Am. J. Hum. Genet. *70*, 1015–1022.
13. Madaule, P., Furuyashiki, T., Reid, T., Ishizaki, T., Watanabe, G., Morii, N., and Narumiya, S. (1995). A novel partner for the GTP-bound forms of rho and rac. FEBS Lett. *377*, 243–248.
14. Watanabe, S., De Zan, T., Ishizaki, T., and Narumiya, S. (2013). Citron kinase mediates transition from constriction to abscission through its coiled-coil domain. J. Cell Sci. *126*, 1773–1784.
15. Camera, P., da Silva, J.S., Griffiths, G., Giuffrida, M.G., Ferrara, L., Schubert, V., Imarisio, S., Silengo, L., Dotti, C.G., and Di Cunto, F. (2003). Citron-N is a neuronal Rho-associated protein involved in Golgi organization through actin cytoskeleton regulation. Nat. Cell Biol. *5*, 1071–1078.
16. Di Cunto, F., Imarisio, S., Hirsch, E., Broccoli, V., Bulfone, A., Migheli, A., Atzori, C., Turco, E., Triolo, R., Dotto, G.P., et al. (2000). Defective neurogenesis in citron kinase knockout mice by altered cytokinesis and massive apoptosis. Neuron *28*, 115–127.
17. Madaule, P., Eda, M., Watanabe, N., Fujisawa, K., Matsuoka, T., Bito, H., Ishizaki, T., and Narumiya, S. (1998). Role of citron kinase as a target of the small GTPase Rho in cytokinesis. Nature *394*, 491–494.
18. Carrera, A.C., Alexandrov, K., and Roberts, T.M. (1993). The conserved lysine of the catalytic domain of protein kinases is actively involved in the phosphotransfer reaction and not required for anchoring ATP. Proc. Natl. Acad. Sci. USA *90*, 442–446.
19. Jacobs, M., Hayakawa, K., Swenson, L., Bellon, S., Fleming, M., Taslimi, P., and Doran, J. (2006). The structure of dimeric ROCK I reveals the mechanism for ligand selectivity. J. Biol. Chem. *281*, 260–268.
20. Kornev, A.P., Haste, N.M., Taylor, S.S., and Eyck, L.F. (2006). Surface comparison of active and inactive protein kinases identifies a conserved activation mechanism. Proc. Natl. Acad. Sci. USA *103*, 17783–17788.
21. Di Cunto, F., Calautti, E., Hsiao, J., Ong, L., Topley, G., Turco, E., and Dotto, G.P. (1998). Citron rho-interacting kinase, a novel tissue-specific ser/thr kinase encompassing the Rho-Rac-binding protein Citron. J. Biol. Chem. *273*, 29706–29711.
22. Green, R.A., Paluch, E., and Oegema, K. (2012). Cytokinesis in animal cells. Annu. Rev. Cell Dev. Biol. *28*, 29–58.
23. Gai, M., Camera, P., Dema, A., Bianchi, F., Berto, G., Scarpa, E., Germena, G., and Di Cunto, F. (2011). Citron kinase controls abscission through RhoA and anillin. Mol. Biol. Cell *22*, 3768–3778.
24. Okita, K., Matsumura, Y., Sato, Y., Okada, A., Morizane, A., Okamoto, S., Hong, H., Nakagawa, M., Tanabe, K., Tezuka, K., et al. (2011). A more efficient method to generate integration-free human iPS cells. Nat. Methods *8*, 409–412.
25. Novarino, G., El-Fishawy, P., Kayserili, H., Meguid, N.A., Scott, E.M., Schroth, J., Silhavy, J.L., Kara, M., Khalil, R.O., Ben-Omran, T., et al. (2012). Mutations in BCKD-kinase lead to a potentially treatable form of autism with epilepsy. Science *338*, 394–397.
26. Gruneberg, U., Neef, R., Li, X., Chan, E.H., Chalamalasetty, R.B., Nigg, E.A., and Barr, F.A. (2006). KIF14 and citron kinase act together to promote efficient cytokinesis. J. Cell Biol. *172*, 363–372.

27. Pilaz, L.J., McMahon, J.J., Miller, E.E., Lennox, A.L., Suzuki, A., Salmon, E., and Silver, D.L. (2016). Prolonged mitosis of neural progenitors alters cell fate in the developing brain. Neuron *89*, 83–99.
28. McIntyre, R.E., Lakshminarasimhan Chavali, P., Ismail, O., Carragher, D.M., Sanchez-Andrade, G., Forment, J.V., Fu, B., Del Castillo Velasco-Herrera, M., Edwards, A., van der Weyden, L., et al.; Sanger Mouse Genetics Project (2012). Disruption of mouse Cenpj, a regulator of centriole biogenesis, phenocopies Seckel syndrome. PLoS Genet. *8*, e1003022.
29. Novorol, C., Burkhardt, J., Wood, K.J., Iqbal, A., Roque, C., Coutts, N., Almeida, A.D., He, J., Wilkinson, C.J., and Harris, W.A. (2013). Microcephaly models in the developing zebrafish retinal neuroepithelium point to an underlying defect in metaphase progression. Open Biol. *3*, 130065.
30. Kaindl, A.M., Passemard, S., Kumar, P., Kraemer, N., Issa, L., Zwirner, A., Gerard, B., Verloes, A., Mani, S., and Gressens, P. (2010). Many roads lead to primary autosomal recessive microcephaly. Prog. Neurobiol. *90*, 363–383.
31. Harding, B.N., Moccia, A., Soukarieh, O., Tubeuf, H., Drunat, S., Chitty, L.S., Verloes, A., Gressens, P., El Ghouzzi, V., Joriot, S., et al. (2016). Mutations in Citron Kinase Cause Recessive Microlissencephaly with Multinucleated Neurons. Am. J. Hum. Genet. *99*, this issue, 511–520.
32. Pearce, L.R., Komander, D., and Alessi, D.R. (2010). The nuts and bolts of AGC protein kinases. Nat. Rev. Mol. Cell Biol. *11*, 9–22.
33. Eda, M., Yonemura, S., Kato, T., Watanabe, N., Ishizaki, T., Madaule, P., and Narumiya, S. (2001). Rho-dependent transfer of Citron-kinase to the cleavage furrow of dividing cells. J. Cell Sci. *114*, 3273–3284.
34. Hauge, C., Antal, T.L., Hirschberg, D., Doehn, U., Thorup, K., Idrissova, L., Hansen, K., Jensen, O.N., Jørgensen, T.J., Biondi, R.M., and Frödin, M. (2007). Mechanism for activation of the growth factor-activated AGC kinases by turn motif phosphorylation. EMBO J. *26*, 2251–2261.
35. Sgrò, F., Bianchi, F.T., Falcone, M., Pallavicini, G., Gai, M., Chiotto, A.M., Berto, G.E., Turco, E., Chang, Y.J., Huttner, W.B., and Di Cunto, F. (2016). Tissue-specific control of midbody microtubule stability by Citron kinase through modulation of TUBB3 phosphorylation. Cell Death Differ. *23*, 801–813.
36. Paramasivam, M., Chang, Y.J., and LoTurco, J.J. (2007). ASPM and citron kinase co-localize to the midbody ring during cytokinesis. Cell Cycle *6*, 1605–1612.
37. Higgins, J., Midgley, C., Bergh, A.M., Bell, S.M., Askham, J.M., Roberts, E., Binns, R.K., Sharif, S.M., Bennett, C., Glover, D.M., et al. (2010). Human ASPM participates in spindle organisation, spindle orientation and cytokinesis. BMC Cell Biol. *11*, 85.
38. Basto, R., Lau, J., Vinogradova, T., Gardiol, A., Woods, C.G., Khodjakov, A., and Raff, J.W. (2006). Flies without centrioles. Cell *125*, 1375–1386.
39. Marjanović, M., Sánchez-Huertas, C., Terré, B., Gómez, R., Scheel, J.F., Pacheco, S., Knobel, P.A., Martínez-Marchal, A., Aivio, S., Palenzuela, L., et al. (2015). CEP63 deficiency promotes p53-dependent microcephaly and reveals a role for the centrosome in meiotic recombination. Nat. Commun. *6*, 7676.
40. Insolera, R., Bazzi, H., Shao, W., Anderson, K.V., and Shi, S.H. (2014). Cortical neurogenesis in the absence of centrioles. Nat. Neurosci. *17*, 1528–1535.

The American Journal of Human Genetics, Volume *99*

Supplemental Data

Biallelic Mutations in Citron Kinase Link Mitotic Cytokinesis to Human Primary Microcephaly

Hongda Li, Stephanie L. Bielas, Maha S. Zaki, Samira Ismail, Dorit Farfara, Kyongmi Um, Rasim O. Rosti, Eric C. Scott, Shu Tu, Neil C. Chi, Stacey Gabriel, Emine Z. Erson-Omay, A. Gulhan Ercan-Sencicek, Katsuhito Yasuno, Ahmet Okay Çağlayan, Hande Kaymakçalan, Barış Ekici, Kaya Bilguvar, Murat Gunel, and Joseph G. Gleeson

Supplemental Data

Supplemental Data include 3 figures and 2 tables.

Figure S1

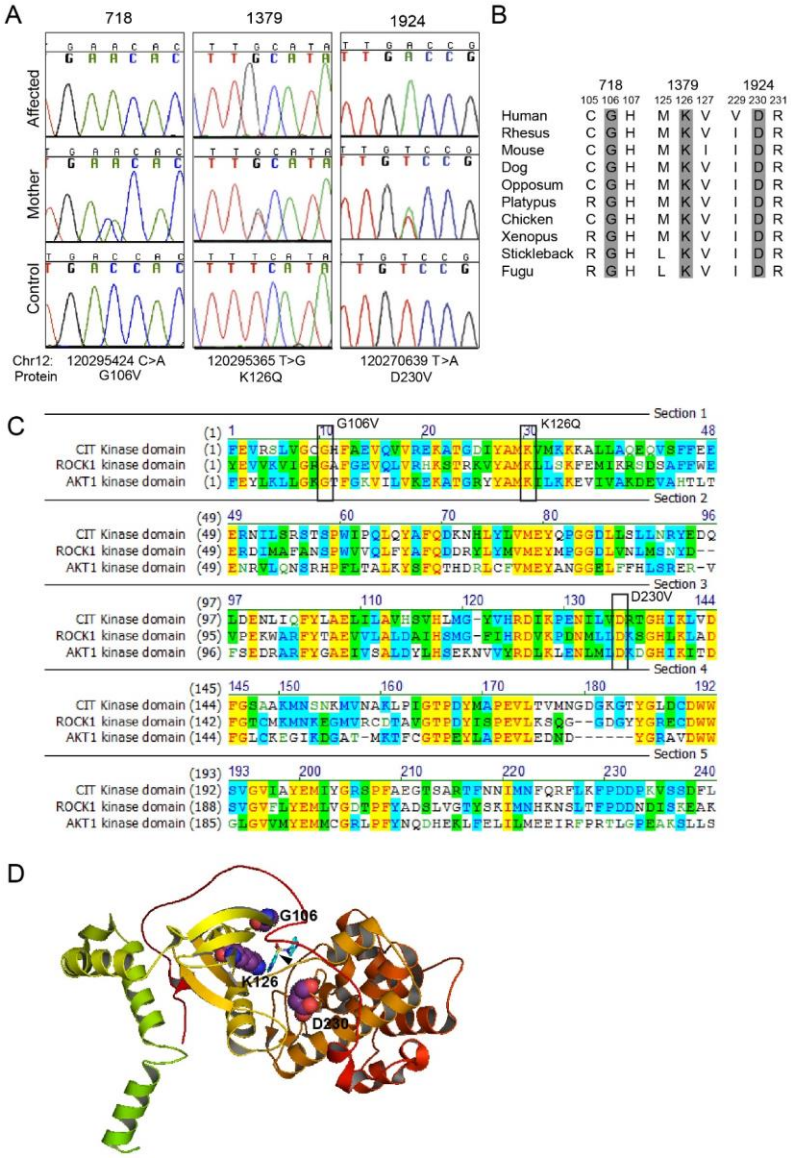

Figure S1. Mutations in the kinase domain of CIT-K cause primary microcephaly
(A) Sequencing chromatograms illustrating *CIT* mutations in the affected children. (B) Evolutionary conservation of the residues with patient mutations across the animal kingdom. (C) Kinase domain conservation among CIT-K and other AGC kinases. The residues with patient mutations are marked with black boxes. The sequence alignment was performed using Vector NTI (Invitrogen). (D) The crystal structure of the kinase domain of ROCK1, with residues with patient mutations labeled. Hydroxyfasudil, a competitive inhibitor of ATP, is marked with arrowhead showing the ATP binding pocket. The kinase domain and residues of ROCK1 were viewed by PyMol (https://www.pymol.org).

Figure S2

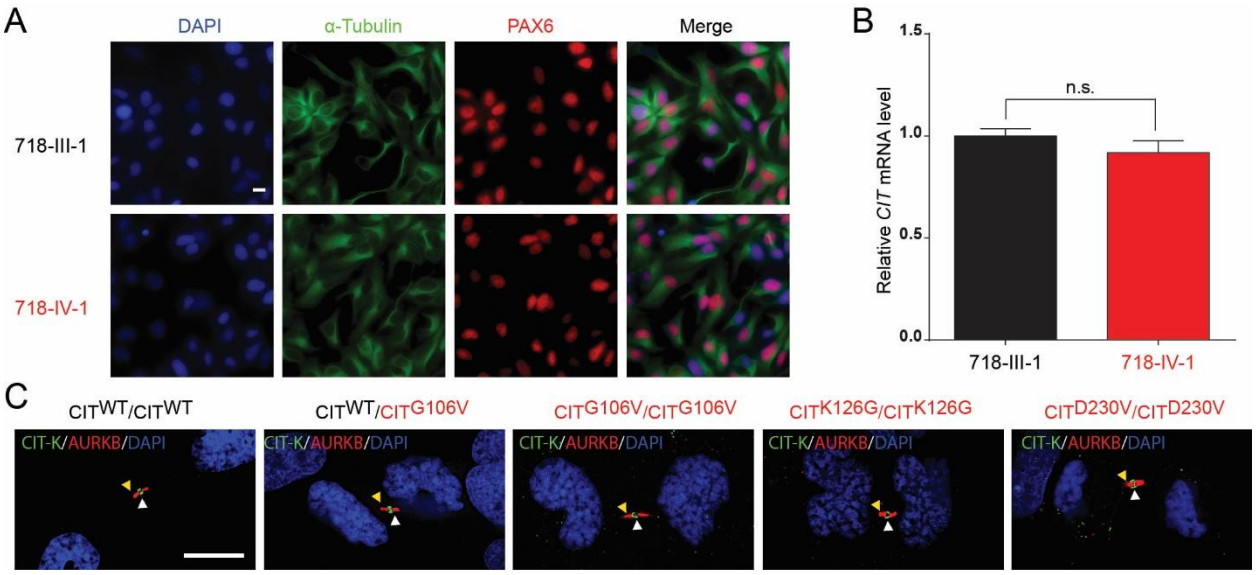

Figure S2. Expression level and localization of CIT-N in patient-derived NPCs
(A) Representative immunocytochemistry images of PAX6+ NPCs differentiated from iPSCs. Scale bar = 10μm. (B) Relative mRNA level of *CIT* in affected and control NPCs. (n=3 cultures for each group). Student's t test. Bar graph: mean ± s.e.m (C) Representative immunocytochemistry images for CIT-K (white arrowhead) and midbody marker Aurora kinase B (AURKB) (yellow arrowhead) during cytokinesis in NPCs with absent, heterozygous or homozygous *CIT* mutations. The localization of CIT-K and AURKB was indistinguishable among all conditions. Scale bar = 10μm.

Figure S3

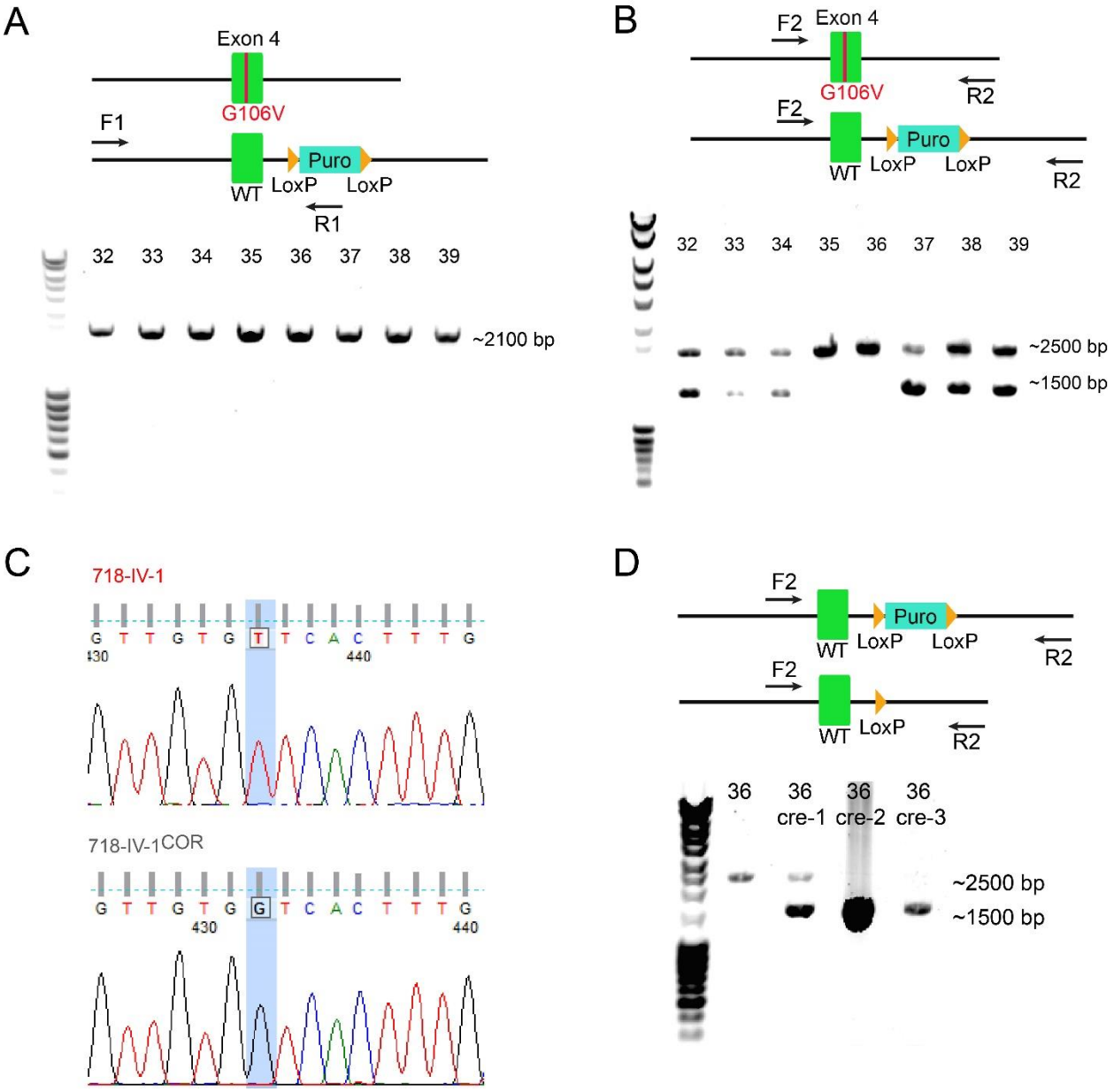

Figure S3. Identification of correctly-targeted iPSC clones in genome editing
(A) Forward primer F1 outside the 5' recombination arm, reverse primer R1 inside the puromycin cassette. This PCR allowed identification of iPSC clones with homologous targeting vector recombination. (B) Forward (F2) and reverse (R2) primers outside of Exon4 and the puromycin cassette. A ~2500 bp band represented the recombined allele, and a ~1500bp band represented the unmodified allele. Clone #35 and #36 were homozygous for homologous recombination, and were chosen for downstream studies. (C) Sanger sequencing confirmed c.317G>T mutation corrected in clone #36. (D) PCR identification of clones with LoxP-Puro-LoxP cassette removal. A ~2500 bp band represented the corrected allele, and a ~1500bp band represented removal of the LoxP-Puro-LoxP cassette. Clone #36-2 and #36-3, with LoxP-Puro-LoxP cassette removal on both alleles, were used for downstream studies.

Table S1 Genetic variants identified in each family from exome sequencing

Family 718

chrom	pos	dbSNP	ref	mut	gene	functionGVS	cDNA Position	AA_Change	PolyPhen Val	SIFTval	CADD PHRED	accession
3	98620028		G	A	DCBLD2	missense	143	PRO/LEU	0.118	0.5	20.6	NM_080927.3
3	112729916	rs115971253	C	T	C3orf17	missense	889	VAL/ILE	0.165	0.08	12.29	NM_015412.3
3	113377150		C	A	KIAA2018	missense	3380	VAL/LEU	0.05	0.05	23	NM_001009899.2
3	122274792		T	C	PARP9	missense	331	ARG/GLY	0.467	0.01	24	NM_031458.2
3	124141662		T	C	KALRN	missense	2540	ILE/THR	0.596	0.02	26.4	NM_003947.4
10	23399192		A	G	MSRB2	missense	241	ASN/ASP	0.051	0.65	11.51	NM_012228.3
10	25313059	rs116200992	G	T	THNSL1	missense	907	ALA/SER	0.169	0.49	11.04	NM_024838.4
10	27389200		C	A	ANKRD26	missense	56	ARG/LEU	0.003	0.72	10.13	NM_014915.2
10	30317861		C	G	KIAA1462	missense	1220	GLY/ARG	0.971	0.01	23.8	NM_020848.2
12	120295424		C	A	CIT	missense	317	GLY/VAL	1	0	32	NM_007174.2
12	122748141	rs114821540	T	G	VPS33A	missense	274	ILE/LEU	0.058	0.89	15.87	NM_022916.4
16	89347612	rs75362060	C	T	ANKRD11	missense	5340	ALA/THR	0.002	0.95	0.024	NM_013275.4

Family 1379

chrom	pos	dbSNP	ref	mut	gene	functionGVS	cDNA Position	AA_Change	PolyPhen Val	SIFTval	PHRED	accession
1	230846446		A	G	AGT	missense	151	CYS/ARG	0.987	0.01	23.7	NM_000029.3
1	234565060		G	A	TARBP1	missense	2882	SER/PHE	0.736	0.04	28.3	NM_005646.3
2	179203724		C	T	OSBPL6	missense	734	ALA/VAL	0.999	0.13	28.2	NM_145739.2
2	179457681	rs116592778	A	G	TTN	missense	32546	VAL/ALA	NA	NA	14.63	NM_133437.3
2	186664898		A	G	FSIP2	missense	11132		0.023	0.02	18.14	
2	231380146	rs61733089	G	A	SP100	missense	2431	ALA/THR	NA	NA	4.163	NM_003113.3
3	73024182		T	C	GXYLT2	missense	1204	PHE/LEU	0.411	1	16.73	NM_001080393.1
4	9336408		A	G	LOC72837	missense	25	ARG/GLY	0	1	0.002	NM_001242328.1
5	75596565		T	C	SV2C	missense	1648	TYR/HIS	0.827	0.5	24.2	NM_014979.1
5	79025441		C	T	CMYA5	missense	853	ARG/CYS	0.046	0.02	13.24	NM_153610.3
5	89930940		G	A	GPR98	missense	1849	VAL/MET	0.038	0.03	23.1	NM_032119.3
5	135513083		A	AT	SMAD5	frameshift	0		0.069	0.12	12.56	
10	103900766	rs17855877	C	G	PPRC1	missense	2501	PRO/ARG	0.787	0.04	23.2	NM_015062.3
10	124091985		A	G	BTBD16	missense	1121	ASP/GLY	0.997	0.02	33	NM_144587.2
10	125521435	rs112981683	T	C	CPXM2	missense	1730	LYS/ARG	1	0.06	23	NM_198148.2
11	78369281		C	T	ODZ4	missense	8132	ARG/GLN	0.013	0.28	23.1	NM_001098816.2
11	111228529	rs35664667	T	C	POU2AF1	missense	181	THR/ALA	0.012	0.46	6.234	NM_006235.2
12	120295365		T	G	CIT	missense	376	LYS/GLN	1	0	26.7	NM_007174.2
12	121853964		G	A	RNF34	ding-synonym	12		NA	NA	16.6	NM_194271.1
14	105417500		C	T	AHNAK2	missense	4288	GLU/LYS	0.086	0.2	3.783	NM_138420.2
20	3804572		G	T	C20orf29	missense	231	MET/ILE	0.003	0.39	10.15	NM_018347.2
20	3843058		C	A	MAVS	missense	623	ALA/GLU	0.522	0.01	23.5	NM_020746.4
21	33694796		C	T	URB1	missense	5332	ASP/ASN	0.127	0.15	22	NM_014825.2
21	37444851		G	C	LOC1001	missense	505		0.05	0.22	20.4	NM_001757.2
21	43287457		TC	T	PRDM15	frameshift	0		NA	NA	12.37	
21	43531659		C	T	UMODL1	missense	2327	PRO/LEU	0.851	0.08	19.24	NM_173568.3

Family 1924

chrom	pos	dbSNP	ref	mut	gene	functionGVS	cDNA Position	AA_Change	PolyPhen Val	SIFT val	PHRED	Accession
2	179440696	rs55853138	C	T	TTN	missense	43568	Arg14448Gln	1	0.006	23.6	NM_133432.3
2	190338924		G	A	WDR75	missense	2122	Glu688Lys	0.998	0.04	35	NM_032168.1
2	190338928		G	A	WDR75	missense	2126	Ser689Asn	0.966	0.313	21.8	NM_032168.1
3	51749962	rs151188856	G	A	GRM2	missense	2412	Asp725Asn	1	0.017	33	NM_000839.3
3	49849583		C	T	UBA7	missense	922	Gly251Arg	0.999	0	25.4	NM_003335.2
12	123444667		C	T	ABCB9	missense	426	Arg39His	0.968	0.138	29.9	NM_019625.3
12	120270639		T	A	CIT	missense	745	Asp230Val	0.98	0	35	NM_001206999.1
12	120884493	rs149168717	C	T	G00000257	missense	158	His39Tyr	0.085	0.454	22.8	NM_176818.2
12	120662133		G	A	PXN	missense	918	Arg19Trp	0.999	0.001	25.1	XM_005253915.1
13	95673848		A	G	ABCC4	missense	4078	Ile1320Thr	0.954	0.002	23.2	NM_005845.3
18	580778		A	G	CETN1	missense	410	Lys124Glu	0.017	0.108	14.51	NM_004066.1
19	41198211	rs144343899	T	C	ADCK4	missense	1431	Tyr455Cys	0.998	0	22	XM_005259272.1
19	41205970		AC	C	ADCK4	splice_donor					27.1	
19	40964447	rs144111604	C	T	BLVRB	missense	195	Glu29Lys	0.013	0.56	25.4	XM_005259157.1
19	47883001	rs200643374	A	G	DHX34	missense	3090	Asn914Ser	0.028	0.145	35	NM_014681.5
19	44536034		C	A	ZNF222	stop_gained	422	Cys109X			11.1	NM_001129996.1
X	79979316		A	C	BRWD3	missense	1844	His527Gln	0.743	0.251	22.9	NM_153252.4
X	131203569		G	A	G00000134	missense	908	Asp221Asn	0.07	0.08	26.5	XM_005262424.1

Abbreviations. Chrom, chromosome; pos, position; ref, reference; mut, mutation.

Table S2 Additional variants identified in 1379-B1-1 from exome sequencing

We identified additional compound heterozygous variants and dominant variants in subject 1379-B1-1.

Compound heterozygous variants

CHROM	POS	effect	gene_name	dbSNP	HGVS_c	HGVS_p	transcript_id	impact
2	201488623	missense_variant	AOX1	rs369839297	c.2041G>A	p.Asp681Asn	ENST00000374700	MODERATE
2	201501730	missense_variant	AOX1	rs144419430	c.2443G>A	p.Gly815Arg	ENST00000374700	MODERATE
6	157488190	missense_variant	ARID1B	rs34786733	c.2857G>A	p.Gly953Ser	ENST00000350026	MODERATE
6	157522223	missense_variant	ARID1B	rs34870395	c.4456A>T	p.Met1486Leu	ENST00000350026	MODERATE
2	29287937	splice_region_variant	C2orf71		c.3669-5_3669-4insCA		ENST00000331664	LOW
2	29287938	splice_region_variant	C2orf71		c.3669-6_3669-5insA		ENST00000331664	LOW
1	17256337	splice_region_variant	CROCC		c.352-4G>A		ENST00000375541	LOW
1	17256531	splice_region_variant	CROCC	rs371339969	c.537+5G>A		ENST00000375541	LOW
1	156499967	missense_variant	IQGAP3	rs149623112	c.4334G>A	p.Arg1445His	ENST00000361170	MODERATE
1	156520100	missense_variant	IQGAP3	rs59573847	c.1778G>T	p.Arg593Leu	ENST00000361170	MODERATE
16	4714702	splice_region_variant	MGRN1	rs199769383	c.562-8C>G		ENST00000262370	LOW
16	4733217	splice_region_variant	MGRN1	rs200737185	c.1483-8T>C		ENST00000262370	LOW
3	195512549	inframe_deletion	MUC4		c.5854_5901delCCTCTT	p.Pro1952_Thr1967del	ENST00000463781	MODERATE
3	195518118	frameshift_variant	MUC4		c.326_332delATGTGAT	p.Asn109fs	ENST00000463781	HIGH
5	141324975	missense_variant	PCDH12	rs3833449	c.3526G>A	p.Gly1176Ser	ENST00000231484	MODERATE
5	141324976	missense_variant	PCDH12	rs13188049	c.3525A>C	p.Arg1175Ser	ENST00000231484	MODERATE
10	3187831	missense_variant	PITRM1	rs34837384	c.2120G>A	p.Arg707Gln	ENST00000451104	MODERATE
10	3214939	missense_variant	PITRM1	rs199766052	c.26G>T	p.Gly9Val	ENST00000380989	MODERATE
9	8331582	frameshift_variant&s	PTPRD	rs200157286	c.4303_4304insT	p.Ser1435fs	ENST00000397611	HIGH
9	8331584	stop_gained&splice_r	PTPRD		c.4302C>A	p.Cys1434*	ENST00000397611	HIGH
19	50037548	missense_variant	RCN3		c.341T>A	p.Ile114Lys	ENST00000270645	MODERATE
19	50040307	missense_variant	RCN3	rs77227069	c.463G>A	p.Val155Met	ENST00000270645	MODERATE
15	42977810	missense_variant	STARD9	rs140924205	c.4034T>G	p.Ile1345Ser	ENST00000290607	MODERATE
15	42978141	missense_variant	STARD9	rs376229251	c.4365A>C	p.Glu1455Asp	ENST00000290607	MODERATE
15	42977810	missense_variant	STARD9	rs140924205	c.4034T>G	p.Ile1345Ser	ENST00000290607	MODERATE
15	42982583	missense_variant	STARD9	rs115491632	c.8807G>T	p.Gly2936Val	ENST00000290607	MODERATE
15	42978141	missense_variant	STARD9	rs376229251	c.4365A>C	p.Glu1455Asp	ENST00000290607	MODERATE
15	42982583	missense_variant	STARD9	rs115491632	c.8807G>T	p.Gly2936Val	ENST00000290607	MODERATE
6	152623062	missense_variant	SYNE1	rs150376715	c.17270C>G	p.Thr5757Arg	ENST00000423061	MODERATE
6	152647218	missense_variant	SYNE1	rs35493783	c.15100G>A	p.Asp5034Asn	ENST00000423061	MODERATE

Abbreviations. Chrom, chromosome; pos, position; ref, reference; mut, mutation; HGVS, Human Genome Variation Society; HGVS_c, cDNA location; HGVS_p, protein location.

Dominant variants

CHROM	POS	effect	gene_nan	dbSNP	HGVS_c	HGVS_p	transcript_id	impact
1	1254762	stop_gained	CPSF3L		c.256A>T	p.Lys86*	ENST00000545578	HIGH
1	120277963	missense_variant	PHGDH		c.689G>A	p.Arg230His	ENST00000369409	MODERATE
1	156499967	missense_variant	IQGAP3	rs149623112	c.4334G>A	p.Arg1445His	ENST00000361170	MODERATE
1	156520100	missense_variant	IQGAP3	rs59573847	c.1778G>T	p.Arg593Leu	ENST00000361170	MODERATE
2	74274744	missense_variant	TET3	rs148646838	c.1295T>C	p.Val432Ala	ENST00000409262	MODERATE
2	110922668	missense_variant	NPHP1	rs113450177	c.503C>T	p.Ala168Val	ENST00000355301	MODERATE
2	152483510	splice_region_variant	NEB	rs141088433	c.10347+6C>T		ENST00000397345	LOW
2	171240217	splice_region_variant	MYO3B	rs146172688	c.1186-3C>T		ENST00000408978	LOW
2	201488623	missense_variant	AOX1	rs369839297	c.2041G>A	p.Asp681Asn	ENST00000374700	MODERATE
3	45049073	splice_region_variant	EXOSC7	rs145650051	c.771+6G>A		ENST00000265564	LOW
3	47452676	missense_variant	PTPN23	rs138329311	c.3388G>A	p.Gly1130Ser	ENST00000265562	MODERATE
3	52430897	missense_variant	DNAH1		c.11624C>T	p.Thr3875Met	ENST00000420323	MODERATE
3	186947662	missense_variant	MASP1		c.1327C>T	p.Arg443Trp	ENST00000337774	MODERATE
5	98115646	stop_gained	RGMB	rs201449079	c.622G>T	p.Gly208*	ENST00000308234	HIGH
5	141324975	missense_variant	PCDH12	rs3833449	c.3526G>A	p.Gly1176Ser	ENST00000231484	MODERATE
5	141324976	missense_variant	PCDH12	rs13188049	c.3525A>C	p.Arg1175Ser	ENST00000231484	MODERATE
6	56342136	splice_region_variant	DST	rs34892827	c.13806+7G>A		ENST00000244364	LOW
6	152623062	missense_variant	SYNE1	rs150376715	c.17270C>G	p.Thr5757Arg	ENST00000423061	MODERATE
6	152623062	missense_variant	SYNE1	rs150376715	c.17483C>G	p.Thr5828Arg	ENST00000367255	MODERATE
6	152647218	missense_variant	SYNE1	rs35493783	c.15100G>A	p.Asp5034Asn	ENST00000423061	MODERATE
6	157488190	missense_variant	ARID1B	rs34786733	c.2896G>A	p.Gly966Ser	ENST00000346085	MODERATE
6	157522223	missense_variant	ARID1B	rs34870395	c.4456A>T	p.Met1486Leu	ENST00000350026	MODERATE
7	12443318	missense_variant	VWDE		c.25G>C	p.Val9Leu	ENST00000275358	MODERATE
7	134719612	missense_variant	AGBL3		c.1270C>T	p.Arg424Cys	ENST00000436302	MODERATE
7	143096736	splice_region_variant	EPHA1	rs149923216	c.835+8C>T		ENST00000275815	LOW
8	33361259	splice_region_variant	TTI2	rs199720231	c.1115+7C>G		ENST00000360742	LOW
8	52384860	missense_variant	PXDNL		c.699C>A	p.Ser233Arg	ENST00000356297	MODERATE
8	120814146	missense_variant	TAF2		c.680A>G	p.His227Arg	ENST00000378164	MODERATE
8	141034062	missense_variant	TRAPPC9		c.2671A>C	p.Thr891Pro	ENST00000438773	MODERATE
8	144995672	missense_variant	PLEC	rs200683827	c.8221G>A	p.Ala2741Thr	ENST00000398774	MODERATE
9	13158047	missense_variant	MPDZ		c.3422C>T	p.Thr1141Ile	ENST00000541718	MODERATE
9	98677946	splice_region_variant	ERCC6L2	rs367808564	c.822-4A>G		ENST00000288985	LOW
9	135940049	missense_variant	CEL		c.249C>A	p.Phe83Leu	ENST00000372080	MODERATE
10	3187831	missense_variant	PITRM1	rs34837384	c.2120G>A	p.Arg707Gln	ENST00000451104	MODERATE
10	3214939	missense_variant	PITRM1	rs199766052	c.26G>T	p.Gly9Val	ENST00000380989	MODERATE
10	32856748	frameshift_variant	CCDC7		c.1351_1354delAC	p.Thr451fs	ENST00000277657	HIGH
10	37433935	missense_variant	ANKRD30A		c.1238C>T	p.Pro413Leu	ENST00000361713	MODERATE
10	60562867	missense_variant	BICC1	rs77500675	c.2046A>T	p.Glu682Asp	ENST00000373886	MODERATE
11	20907067	missense_variant	NELL1	rs115437355	c.584A>G	p.Gln195Arg	ENST00000357134	MODERATE
11	34129870	inframe_insertion	NAT10	rs139367378	c.100_102dupAAA	p.Lys34dup	ENST00000257829	MODERATE
11	46766098	missense_variant	CKAP5		c.5554G>A	p.Val1852Met	ENST00000312055	MODERATE
11	62656158	missense_variant	SLC3A2	rs201220940	c.1583C>T	p.Ala528Val	ENST00000338663	MODERATE
11	65487790	inframe_deletion	RNASEH2(	rs141875736	c.268_270delAAG	p.Lys90del	ENST00000308418	MODERATE
12	57864531	missense_variant	GLI1	rs138680284	c.1624G>T	p.Ala542Ser	ENST00000543426	MODERATE
12	103246735	splice_region_variant	PAH	rs62508624	c.707-7A>T		ENST00000553106	LOW
12	109702166	missense_variant	ACACB	rs149917930	c.6917G>A	p.Arg2306Gln	ENST00000338432	MODERATE
13	25479878	missense_variant	CENPJ	rs79951875	c.2298T>A	p.Asp766Glu	ENST00000381884	MODERATE
13	44454253	splice_region_variant	LACC1	rs73465585	c.-37C>A		ENST00000325686	LOW
15	42977810	missense_variant	STARD9	rs140924205	c.4034T>G	p.Ile1345Ser	ENST00000290607	MODERATE
15	42978141	missense_variant	STARD9	rs376229251	c.4365A>C	p.Glu1455Asp	ENST00000290607	MODERATE
15	42982583	missense_variant	STARD9	rs115491632	c.8807G>T	p.Gly2936Val	ENST00000290607	MODERATE
15	75644499	missense_variant	NEIL1		c.482T>C	p.Ile161Thr	ENST00000355059	MODERATE
15	84506964	missense_variant	ADAMTSL	rs112527144	c.724A>G	p.Lys242Glu	ENST00000286744	MODERATE
16	27715275	missense_variant	KIAA0556	rs143325975	c.1345G>A	p.Gly449Ser	ENST00000261588	MODERATE
16	56875738	missense_variant	NUP93	rs147381896	c.1973G>A	p.Arg658His	ENST00000564887	MODERATE
16	67298319	missense_variant	SLC9A5		c.1907T>G	p.Val636Gly	ENST00000299798	MODERATE
16	71571175	missense_variant	CHST4	rs141141955	c.595C>T	p.His199Tyr	ENST00000338482	MODERATE
17	649703	missense_variant	GEMIN4		c.1580A>G	p.Asn527Ser	ENST00000319004	MODERATE
17	7671259	missense_variant	DNAH2	rs146539788	c.3717C>A	p.Asp1239Glu	ENST00000389173	MODERATE
17	16068429	missense_variant	NCOR1		c.155C>T	p.Ser52Leu	ENST00000395848	MODERATE
17	62024398	splice_region_variant	SCN4A	rs142270113	c.3441+7G>A		ENST00000435607	LOW
19	8161433	missense_variant	FBN3	rs115948457	c.5434A>G	p.Ile1812Val	ENST00000270509	MODERATE
19	9868536	frameshift_variant	ZNF846		c.1213_1216delAA	p.Asn405fs	ENST00000397902	HIGH
19	18256548	splice_region_variant	MAST3	rs73925428	c.2953-5C>T		ENST00000262811	LOW
19	50037548	missense_variant	RCN3		c.341T>A	p.Ile114Lys	ENST00000270645	MODERATE
19	50040307	missense_variant	RCN3	rs77227069	c.463G>A	p.Val155Met	ENST00000270645	MODERATE